MOEM

Modern Electronic Materials 2019; 5(2): 51–60
DOI 10.3897/j.moem.5.2.51314

Research Article

Tailoring of stable induced domains near a charged domain wall in lithium niobate by probe microscopy

Alexander M. Kislyuk[1], Tatiana S. Ilina[1], Ilya V. Kubasov[1], Dmitry A. Kiselev[1], Alexander A. Temirov[1], Andrei V. Turutin[1], Mikhail D. Malinkovich[1], Andrey A. Polisan[1], Yury N. Parkhomenko[1,2]

1 National University of Science and Technology MISiS, 4 Leninsky Prospekt, Moscow 119049, Russia

2 JSC "Giredmet", 2 Elektrodnaya Str., Moscow 111524, Russia

Corresponding author: *Alexander M. Kislyuk* (akislyuk94@gmail.com)

Received 26 December 2018 ♦ **Accepted** 23 February 2019 ♦ **Published** 1 June 2019

Citation: Kislyuk AM, Ilina TS, Kubasov IV, Kiselev DA, Temirov AA, Turutin AV, Malinkovich MD, Polisan AA, Parkhomenko YuN (2019) Tailoring of stable induced domains near a charged domain wall in lithium niobate by probe microscopy. Modern Electronic Materials 5(2): 51–60. https://doi.org/10.3897/j.moem.5.2.51314

Abstract

Ferroelectric lithium niobate ($LiNbO_3$) crystals with an engineered domain structure have a number of applications in optical systems for generation of multiple laser radiation harmonics, acoustooptics, precision actuators, vibration and magnetic field sensors, including those for high-temperature applications, and prospectively, in non-volatile computer memory. We have studied the effect of charged domain boundary on the formation of induced domain structures in congruent lithium niobate ($LiNbO_3$) crystals at the non-polar *x*-cut. Bi- and polydomain ferroelectric structures containing charged "head-to-head" and "tail-to-tail" type domain boundaries have been formed in the specimens using diffusion annealing in air ambient close to the Curie temperature and infrared annealing in an oxygen free environment. The surface potential near the charged domain wall has been studied using an atomic force microscope (AFM) in Kelvin mode. We have studied surface wedge-shaped induced microscopic domains formed at the charged domain boundary and far from that boundary by applying electric potential to the AFM cantilever which was in contact with the crystal surface.

We have demonstrated that the morphology of the induced domain structure depends on the electrical conductivity of the crystals. The charged "head-to-head" domain boundary has a screening effect on the shape and size of the domain induced at the domain wall. Single wedge-shaped domains forming during local repolarization of reduced lithium niobate crystals at the AFM cantilever split into families of microscopic domains in the form of codirectional beams emerging from a common formation site. The charged domain wall affects the topography of the specimens by inducing the formation of an elongated trench, coincident with the charged boundary, during reduction annealing.

Keywords

lithium niobate, bidomain crystal, charged domain wall, diffusion annealing, atomic piezoresponse force microscopy, surface potential

1. Introduction

Ferroelectric lithium niobate ($LiNbO_3$) crystals with an engineered domain structure have a number of applications in optical systems for generation of multiple laser radiation harmonics, acoustooptics, precision actuators, vibration and magnetic field sensors, including those for high-temperature applications, and prospectively, in non-volatile com-

puter memory [1–12]. Despite the availability of proven technologies of growth of the crystals with required ferroelectric domain structures and devices on their basis, researchers draw much attention to the fundamental properties of domain structures, their technologies, formation kinetics and description at micro- and macroscopic levels [13–17].

Since lithium niobate is a 180° (or so called uniaxial) ferroelectric it can contain three types of domain boundaries: "head-to-tail", "head-to-head" and "tail-to-tail" type ones [18, 19]. In the former type of domain boundaries the line separating the two adjacent domains is parallel to their spontaneous polarization vectors. Head-to-tail domain boundaries have moderate free energy since they are either uncharged or weakly charged. On the contrary, "head-to-head" and "tail-to-tail" domain boundaries are arranged at a nearly 90° angle to the spontaneous polarization vectors of the adjacent domains and therefore have their own bound charge (positive for head-to-head boundaries and negative for tail-to-tail ones). This charge increases the free energy of the crystal and is compensated by mobile carriers causing local changes in the electrophysical properties near the domain boundaries.

The formation of a charged domain walls in a crystal is not advantageous from the energy viewpoint. However, polydomain ferroelectric crystals that were cooled for sufficiently long time and underwent a paraelectric to ferroelectric phase transition always contain head-to-head and tail-to-tail domain boundaries or close ones. There are methods of increasing the concentration of charged domain boundaries. It was shown that lithium niobate and lithium tantalate crystals can be polarized so that only one long domain boundary exists in the whole crystal bulk that splits two domains and is oriented, at a macroscopic scale, orthogonally to the spontaneous polarization direction. Methods of synthesizing these bidomain structures imply the formation of an inner force field in the crystal bulk associated with a temperature gradient [20–24] or a concentration gradient [25–31] during a paraelectric to ferroelectric phase transition. Since the abovementioned processes occur at high temperatures (~1100 °C), the domain boundary morphology is largely affected by free carriers which can screen the electric field of charged domain walls and reduce their free energy. This seems to be the origin of the more serrated boundary pattern in bidomain $LiTaO_3$ crystals as compared to $LiNbO_3$ crystals as seen in a microscopic level: the lower Curie temperature implies a moderate bulk electrical conductivity during the phase transition and hence a larger number of head-to-tail boundaries [23].

The situation is different for domain formation and growth in bi- and polydomain crystals at low temperatures, e.g. as a result of local repolarization by an external electric field. The extremely low concentration of intrinsic carriers reduces the efficiency of bulk screening in large single-domain regions. However, higher or lower intrinsic carrier concentrations at charged domain walls should cause the formation of new domains with structures differing from that of the single-domain region. Moreover, the intrinsic electric fields of the adjacent domains may give an additional contribution in the local electric field. An unusual behavior of domains at a charged domain wall in lithium niobate crystals was observed earlier: the sign of a needle-shaped domain changed to the opposite when passing through such a boundary [24].

An experimental method for obtaining data on the domain structure and modifying it *in situ* is piezoresponse force microscopy **(PFM)** which is an optional mode available in atomic force microscope **(AFM)**. Applying electric potential to the microscope cantilever one can locally polarize even ferroelectric materials with a high switching field such as $LiNbO_3$. There are multiple indications that ferroelectric domains forming in lithium niobate crystals due to polarization have complex shapes depending on a number of factors: crystallographic orientation of specimen, magnitude and time of voltage application to probe, method of probe movement on specimen surface, electrical conductivity of specimen, surface layer quality and ambient conditions [32–38]. The complex pattern of domain formation is caused by the fundamental instability of charged domain boundaries forming due to electric potential application to the cantilever: the room temperature electrical conductivity of the crystal is low and the field of the growing domain has not sufficient time for being screened by bulk carriers. This causes the formation of relatively shallow domains and increases the free energy of the cantilever and the domain boundary. The competition of these processes and the presence of external factors cause the formation of differently shaped domain structures [32].

The aim of this work is to study local polarization in lithium niobate crystals under atomic force microscope probe in the vicinity of the charged domain boundary.

2. Experimental

We used commercially available lithium niobate crystal plates of congruent composition (cuts *z* and *y* + 128°). The plates were cut into 10 × 10 × 0.5 mm^3 rectangles and a head-to-head bidomain ferroelectric structures were formed by diffusion annealing in air [25, 26, 29]. The Curie temperature of the crystals was 1138 ± 2 °C according to differential scanning calorimetry. After the bidomain structure was formed, two *z*-cut specimens were heat treated in an oxygen free environment for increasing electrical conductivity (the so-called reduction annealing). One specimen was fast annealed at above the Curie point (1150 °C) for the formation of a polydomain ferroelectric structure and the other one was annealed for 100 min at 1050 °C for increasing electrical conductivity in the bidomain crystal. The specimens were annealed in an ULVAC VHC-P610 infrared furnace in a dry nitrogen atmosphere. The electrical conductivity of the reduced crystals was at least 10^{-8} $Ohm^{-1} \times cm^{-1}$ according to fast measurement of reference specimens with a laboratory multimeter; this result is in agreement with literary data [39, 40]. We assumed that the electrical conductivity of the as-cut specimens (before reduction annealing) was 10^{-18} $Ohm^{-1} \cdot cm^{-1}$.

For AFM studies with the method described earlier [22, 24] we prepared thin transverse cuts of the crystals so the polar axis *z* was in the specimen plane and the perpendicular non-polar axis *x* was orthogonal to the crystal surface. The specimen preparation sequence is shown in Fig. 1. After crystal thinning and polishing we glued them onto a metallic substrate with conductive silver paste.

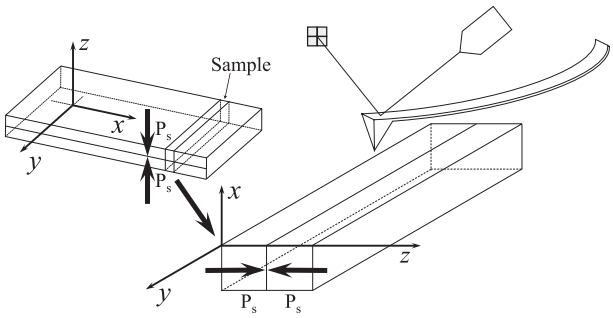

Figure 1. Schematic of specimen preparation for studies.

Data on the test crystals are summarized in Table 1.

in which the charged domain boundary can change the electrophysical properties of the material we studied the specimens in Kelvin mode (Fig. 2). Analysis of the data showed that both in the #Z_HH specimen without reduction annealing and in the #Z_HH_B specimen, the surface potentials at the domain boundary are distributed inhomogeneously. In both crystals the potentials at the boundary are higher than the background ones which agrees with earlier experimental data [41]. The contrast of the charged domain boundary in scans obtained in Kelvin mode is better in the crystal that was not reduction annealed (Fig. 2*b*) probably due to the lower electrical conductivity of that crystal. The width of the region with changed surface potential is 20 μm in the unannealed crystal and 2 μm in the reduction annealed one.

Study of the surface topography for the #Z_HH_B specimen showed that annealing of the *x*-cut crystal in an oxygen free environment caused the formation of an elongated trench on the crystal surface which coincided with the charged domain wall in the PFM scan (Fig. 3). The depth and width of the trench are approx. 0.5 nm and 1 μm, respectively. Below we will discuss possible

Table 1. Parameters of test lithium niobate crystals.

Specimen	Bidomain structure formation	Reduction annealing	Domain structure
#X_SD	–	–	Monodomain
#Y128_HH	Air annealing at 1140 °C for 120 min	–	Head-to-head bidomain
#Z_HH		–	
#Z_HH_B		Annealing in 6.0 grade dry nitrogen atmosphere at 1050 °C for 100 min	
#X_PD_B	–	Annealing in 6.0 grade dry nitrogen atmosphere at 1150 °C for 5 min	Polydomain

Local polarization of ferroelectric domains, study of forming domain structures and measurement of surface potential signal were carried out under a MFP-3D Stand Alone scanning probe microscope (**SPM**) (Asylum Research, USA) with Asyelec-01 cantilevers (Asylum Research, USA) in PFM mode and in Kelvin mode. For domain polarization we applied electric potential to the cantilever relative to earthed substrates with glued-on specimens. Among lithium niobate crystal cuts with a lateral position of the polar axis *z*, the highest threshold switching field and hence the shortest growing domain were observed in the *x*-cut crystals [33, 34]. Therefore we applied high electric potentials to the cantilever (160 to 200 V). All the experiments were carried out at room temperature without stabilization of humidity or illumination in the scanning area. In the PFM images of the domain structure the dark color regions correspond to the left-hand direction of the spontaneous polarization and the bright regions correspond to the right-hand direction of the spontaneous polarization.

3. Results and discussion

To determine the charge state of crystal surface at domain boundaries and evaluate the width of the region

origins of this trench.

Many authors observed earlier [32, 42, 43] that the shape, length and configuration of the forming domains may vary depending on the method of local repolarization in $LiNbO_3$ crystals with the SPM cantilever. For example, it was reported that the induced domain structure depends on the method of probe movement relative to the crystal surface. If the probe remained in contact with the specimen surface while moving between the polarization points the spontaneous polarization vectors of the forming domains were directed against the cantilever electric field [32], and additional micro- and nanodomains formed along the cantilever route [42, 43]. These observations were only made if the cantilever potential was negative. If the cantilever was lifted above the crystal surface before moving to the next polarization point the directions of the spontaneous polarization vectors of the forming domains coincided with the cantilever electric field direction, and no additional nanodomains formed along the cantilever route.

To determine the effect of cantilever contact with the specimen surface during moving between polarization points on the morphology of the polarized domains we studied domains obtained under different conditions. In the #Y128_HH specimen, 10 domains were polarized at the domain boundary to the right and to the left far from

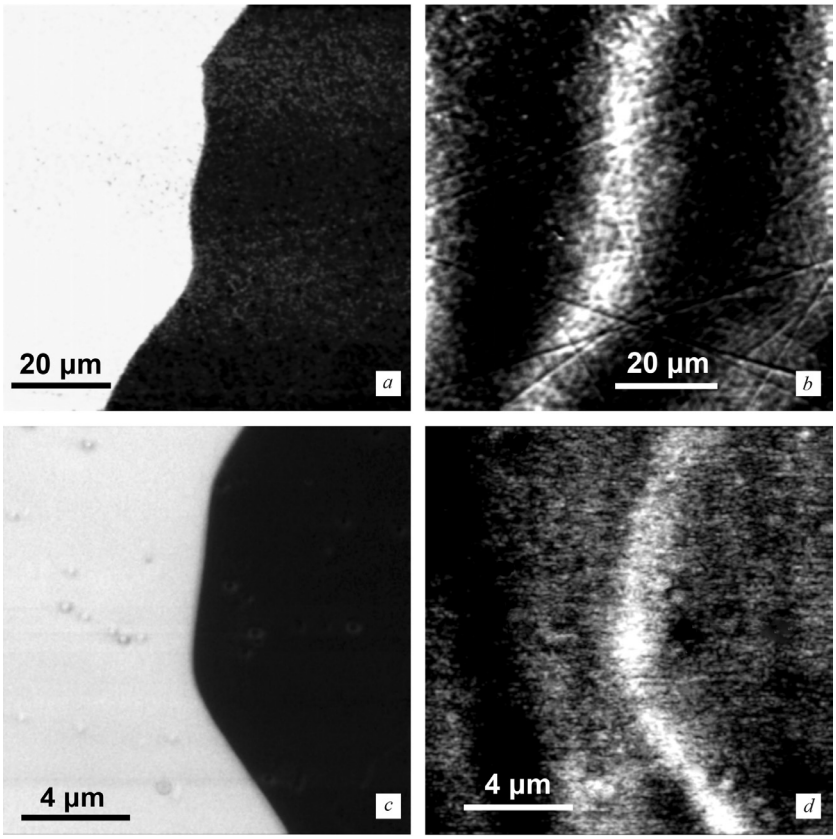

Figure 2. Visualization of head-to-head type charged domain boundary in (*a* and *b*) #Z_HH and (*c* and *d*) #Z_HH_B specimens (*a* and *c*) in piezoelectric force microscopy mode and (*b* and *d*) in Kelvin mode.

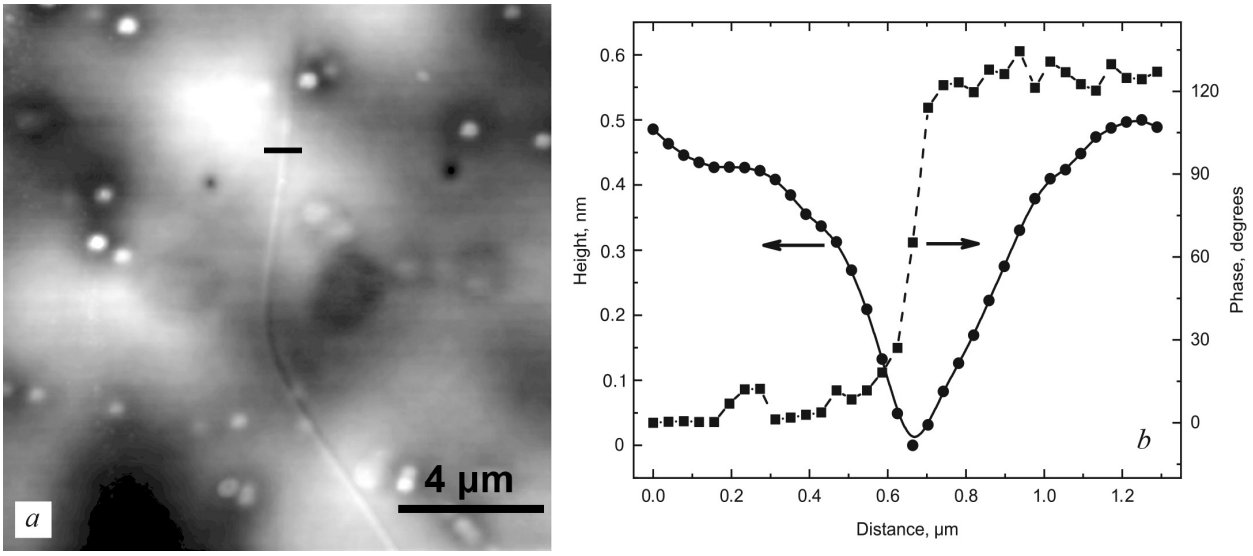

Figure 3. Change in surface topography at charged domain boundary in #Z_HH_B specimen: (*a*) topography, (*b*): (*1*) surface profile and (*2*) piezoresponse phase chart along the section shown in figure.

it with a positive or negative cantilever potential of 200 V for different durations (Fig. 4 *a–f*). Applying a positive potential for 10 s or more produced a complex polarized domain structure which contained an elongated domain the spontaneous polarization direction of which coincided with that of the applied electric field (main domain) and two small (additional) domains that were symmetrical relative to the potential application point, the spontaneous polarization of which was directed against the electric field. Increasing the time of applying positive potential broadened and lengthened the main domain and changed the shape of the additional domains but slightly.

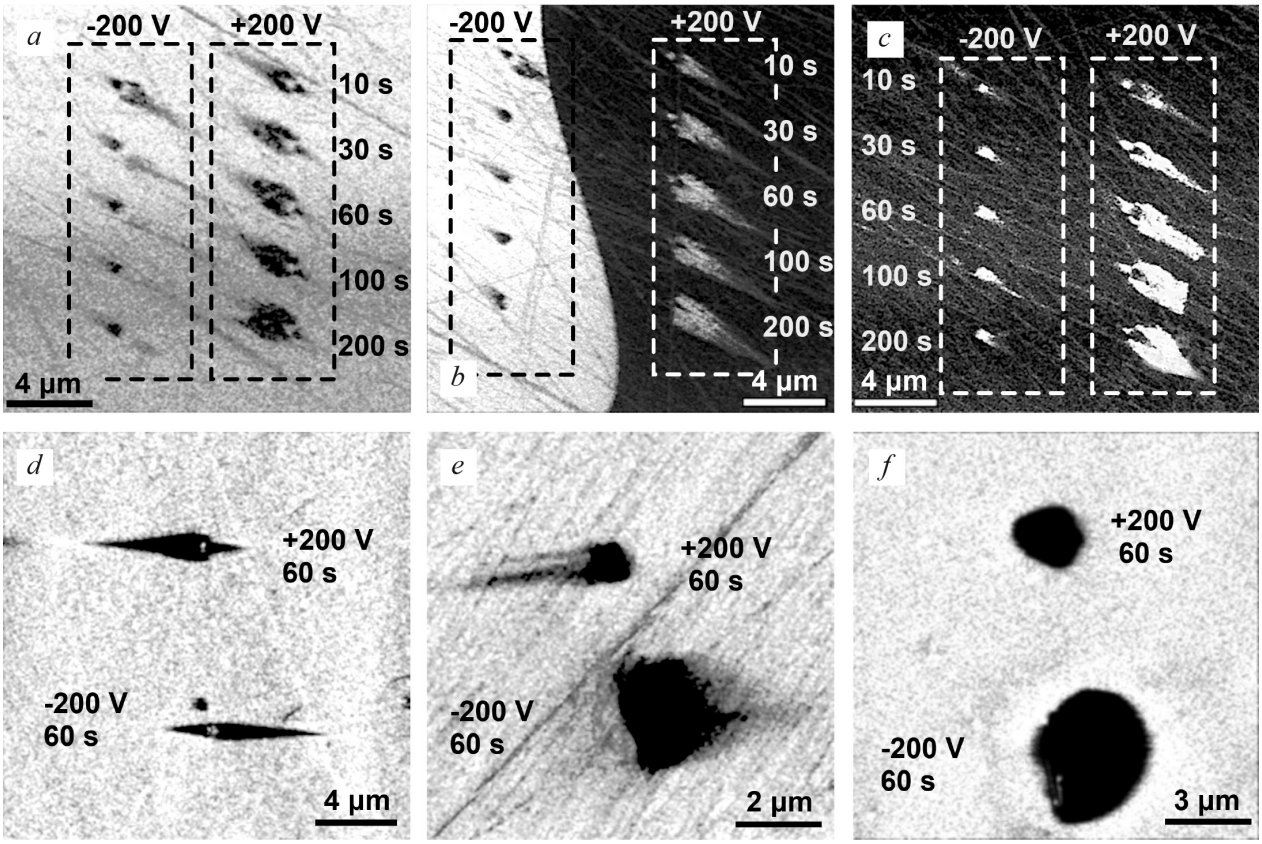

Figure 4. Domains formed in $LiNbO_3$ crystals by (*a–c*) cantilever contacting with crystal surface and (*d–f*) cantilever lifter above crystal surface while moving between points: (*a–c*) #Y128_HH specimen: (*a*) left, (*b*) at and (*c*) right of domain boundary, (*d*) #X_SD specimen, (*e*) monodomain region of #X_PD_B specimen and (*f*) #Z_HH_B specimen. Potential application duration is shown on scans.

Application of a negative potential with the same amplitude as above produced two types of domain structures. If the application time was short (~10 s) the morphology of the complex domain structure was close to that for positive potential (one main and two additional domains). Increasing the cantilever electric field exposure time (30 s or more) completely removed the main domain and one additional domain and caused a slight growth of the second additional domain the spontaneous polarization of which was directed against the cantilever electric field. Microdomains did not form along the cantilever route whether the potential was positive or negative. Our polarization results for contacting cantilever movement between polarization points agree with earlier data [32] for *y*-cut crystals and can be accounted for by different screening rates of electric fields induced in the crystal and in the surface region by positive and negative cantilever electric potentials.

The pattern was different if the cantilever was lifted above the crystal surface while moving to the next polarization point. Then the growth directions of needle-shaped domains coincided with the cantilever electric field direction whether the potential was positive or negative (Fig. 4 *d–f*). With an increase in the electrical conductivity of the crystal which depends on the time and temperature of reduction annealing the role of mobile carriers in screening of the cantilever electric field increases. This causes smearing of the domains polarized by the cantilever and makes their shapes almost round. Unlike the initial (not reduction annealed) crystal in which induced domains have close linear sizes, the area of domains polarized by negative cantilever potential in specimens after reduction annealing was 3–4 that of domains polarized by positive cantilever potential. This can be accounted for by contact phenomena between the cantilever material and lithium niobate or by differences in the mobilities and concentrations of carriers with effective positive and negative charge sign.

Polarization with cantilever lifting without exposure produces domain structures having a stronger contrast and a visually resolvable end of beam. However if this method is used the polarization of adjacent points takes more time as compared to polarization with a contacting cantilever. This shifts the polarization points relative to one another and to the domain boundary due to an imperfect scanning probe microscope positioning system.

Induced domain structures were stable in time and remained unchanged several days after polarization whether the cantilever was contacting or lifted while moving between polarization points.

Study of domain formation under cantilever electric field in polydomain crystal #X_PD_B showed that depending on domain boundary type (head-to-head or tail-to-

tail) the domain grew in different manners if potential was applied directly to the domain boundary. For positive polarization at a head-to-head boundary and negative polarization at a tail-to-tail boundary, the new domain growth was slight if any (Fig. 5 *a, d*). This can be accounted for by the same direction of the cantilever electric field and the spontaneous polarization vector in each adjacent domain. The growth of induced domains at a tail-to-tail domain boundary in case of negative cantilever potential occurred similarly. Then the cantilever electric field was directed against the spontaneous polarization vectors of the adjacent domains and therefore the area of the repolarized region increased twofold (Fig. 5*b*).

The growth of induced domains at a head-to-head domain boundary in the case of positive cantilever potential occurred differently. Then two oppositely directed submicron sized domains formed, and the area of the polarized region did not exceed twofold the induced domain area in the single-domain region. The domain wall was the barrier for needle-shaped domain propagation to adjacent macrodomains (Fig. 5 *c*). The sizes of the induced domains were within 1 μm. Note that there were no traces of formation of the domain with a twofold greater area for either phased or amplitude lateral piezoresponse signals.

Comparison of the shapes of domains forming in non-reduced and reduced lithium niobate crystals showed that under specific conditions one needle-shaped domain can split into a family of adjacent parallel narrow wedge-shaped domains (beams) emerging from a common formation site. Examples of this domain growth are shown in Fig. 4 *e* and in Fig. 6. This multi-beam growth pattern was only observed in reduced lithium niobate crystals, the domain beams being the more the longer was the oxygen-free environment reduction. The length of individual beams emerging from the domain is generally larger in local polarization regions where the cantilever potential was negative. It is safe to assume that this phenomenon is associated with the bulk electric field screening in the cantilever/crystal contact region.

The induced domain grew in bidomain crystals along the boundary, but after some minimum distance between the potential application point and the charged domain wall (~4 μm) a symmetrical semicircle-shaped domain grew in the direction from the boundary towards the wedge-shaped domain polarized by the cantilever (Figs 5 *b*, 6 *d*). The spontaneous polarization vector of the induced domain had the same direction as the cantilever electric field.

The morphology of the domain structure induced by local polarization of ferroelectric domains on non-polar *x*-cuts of $LiNbO_3$ crystal surfaces with the AFM cantilever depends on a number of intrinsic and extrinsic factors. The intrinsic factors include crystal electrical conductivity, surface quality, potential application time, cantilever electric field direction; the extrinsic factors can be experimental conditions (temperature, humidity) and method of experiment (contact or contactless cantilever movement between voltage application points). If the test crystal is not single-domain these factors additionally include the effect of charged head-to-head and tail-to-tail domain boundaries.

Charged domain boundaries in bi- or polydomain crystals are surrounded by regions of changed surface potential. The width of these regions may vary from 20 μm in insulating crystals (without annealing in an oxygen free environment) to 2 μm in highly electrically conductive specimens. The largest difference in electrophysical properties is observed between the crystal bulk and the domain boundary where according to literary data [41] the surface potential is the highest at the head-to-head boundaries and the lowest at the tail-to-tail ones.

The room temperature electrical conductivity of undoped lithium niobate crystals is 10^{-15}–10^{-18} $Ohm^{-1} \times cm^{-1}$. Reduction annealing increases the electrical conductivity to about 10^{-7}–10^{-8} $Ohm^{-1} \times cm^{-1}$ [39, 40, 44]. The electrical conductivity of a charged domain wall differs from that of a single-domain region and may reach 10^{-2} $Ohm^{-1} \times cm^{-1}$ in magnesium doped crystals which is ~13 orders of magnitude higher than the dark electrical conductivity of as-grown congruent lithium niobate [45]. Note that literary data on the electrical conductivity of domain boundaries in thermally reduced lithium niobate crystals are very scarce. The wide range of possible electrical conductivity, anisotropy of physical properties and the difference between the electrical conductivities of the bulk and the surface entail polarization of differently shaped and sized domains in the crystals.

During local polarization of domains in a single-domain specimen or a single-domain region in a bidomain specimen, even a small number of free carriers remaining in the material at room temperature can partially screen the cantilever electric field and lead to the formation of asymmetrical domains that are known from microscopic studies [32] of 180° ferroelectrics. The induced domain has a typical wedge shape and is elongated along the optical axis. This phenomenon is also observed close to the domain boundary. The effect of an increase in electrical conductivity (due to reduction annealing) on the induced domain structure shows itself as a change in the shape of the forming domain from elongated needle-shaped to smeared and close to round (Fig. 4). The high concentration of carriers (in thermally reduced $LiNbO_3$ crystals these carriers are polarons [40, 46–50]) provides for a more efficient screening of the cantilever electric field and elimination of additional domains. The latter form in insulating (unannealed) $LiNbO_3$ due to the secondary polarization of slowly dissipating surface charge. With an increase in the electrical conductivity of the crystals the single beam shaped domain emerging from the electric field application point splits gradually first into 3–4 shorter beams and, with a further growth in carrier concentration, into 5 or more beams. Individual beams can even be resolved at the edges of semicircle-shaped domains forming during local polarization of specimens after long-term heat treatment in an oxygen free environment and seem to efficiently minimize the free energy of the induced domain boundary.

The sizes and shapes of the domains forming after AFM cantilever application directly to a charged domain wall depend on the type and sign of the applied voltage. If the electric field direction is the same as that of the spon-

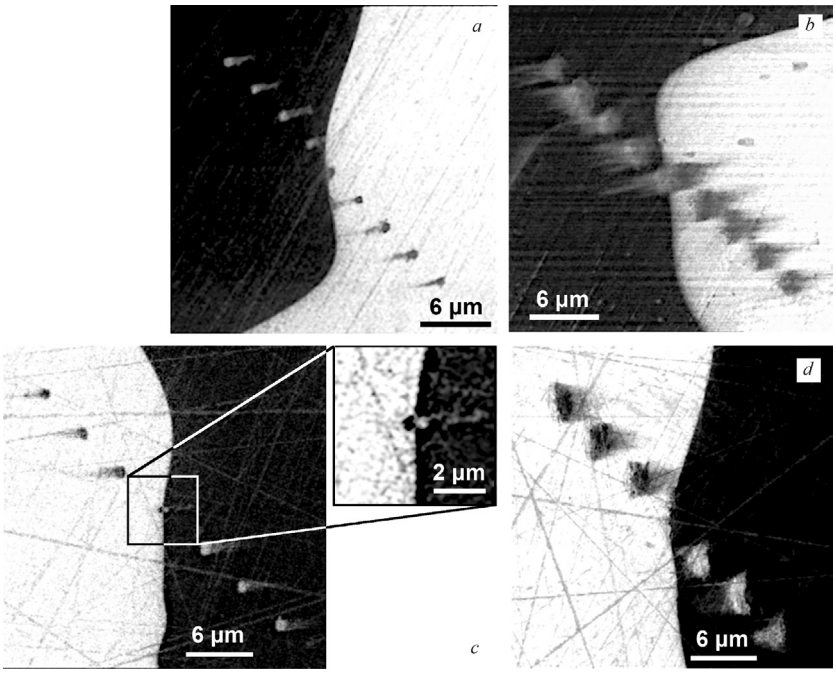

Figure 5. Matrices of induced domains formed in #X_PD_B crystal at charged (*a* and *b*) tail-to-tail and (*c* and *d*) head-to-head domain boundary for (*a* and *c*) positive and (*b* and *d*) negative 200 V potential applied for 60 s.

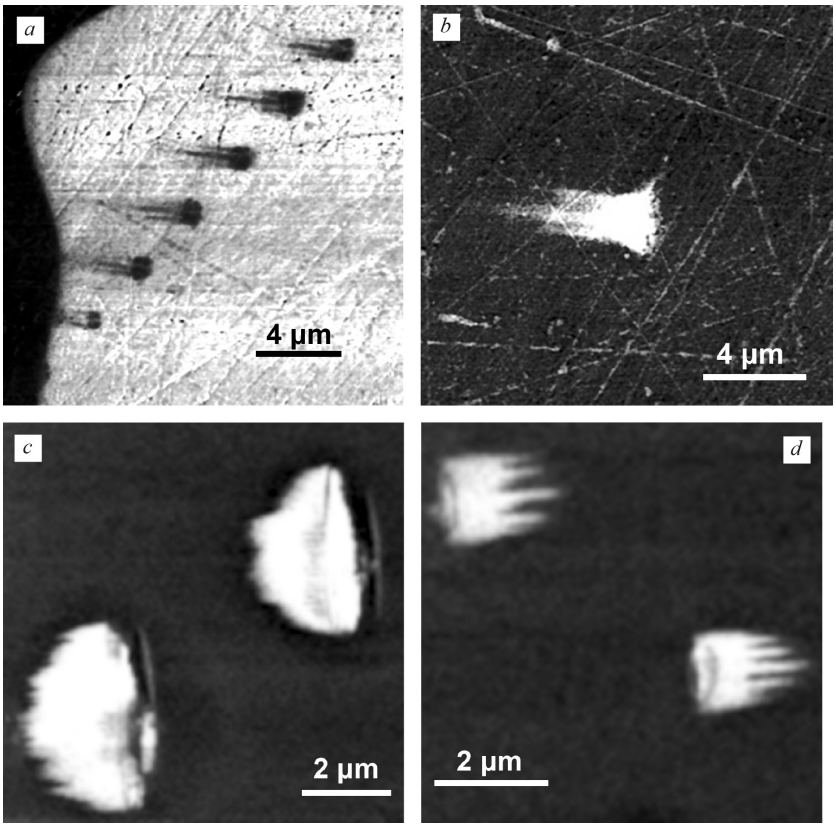

Figure 6. Multi-beam domains induced by applying (*a* and *c*) positive and (*b* and *d*) negative 160 V potential to cantilever for $LiNbO_3$ crystals thermally reduced in an oxygen free environment (*a* and *b*) for 5 min at 1150 °C and (*c* and *d*) for 100 min at 1050 °C.

taneous polarization vectors in the adjacent domains the induced domains do not grow, predictably. If the cantilever electric field direction is directed against the spontaneous polarization vectors of the adjacent macrodomains, the forming domain structure depends on the type of the existing domain boundary. In tail-to-tail structures the induced domain propagates to both sides of the boundary forming a large repolarized region. On the contrary, at

head-to-head boundaries domains grow but slightly (the linear size of the repolarized region is within 1 μm for 200 V voltage applied for 60 s). This can be caused by the much efficient screening of the cantilever electric field by head-to-head domain boundaries due to higher electron concentrations in nearby regions. This elevated carrier concentration is accounted for by the fact that a head-to-head domain structure couples the ends of spontaneous polarization vectors of adjacent domains, i.e., the Li^+ cations in the oxygen octahedrals of the unit cells. The compensation of the double layer of positive charges by bulk electrons increases the electrical conductivity of head-to-head domain boundaries. This was confirmed experimentally earlier [41] using conductive atomic force microscopy. Carrier mobility in a reduced $LiNbO_3$ crystal with a Debye length of 1 μm and an electrical conductivity of 10^{-8} $Ohm^{-1} \times cm^{-1}$ for electron or polaron conductivity is $\mu \sim 10^{-3}$ $cm^2/(V \times s)$ at a free carrier concentration of $\sim 10^{14}$ cm^{-3}. This estimate is in a good agreement with earlier Hall carrier mobility data obtained for similar specimens at room temperature [44]. A tail-to-tail domain structure is a double layer of negative charges in a crystal structure and is not resolvable by conductive AFM [41]. These structures seem not to accumulate high concentration of free negative carriers and hence do not screen the cantilever electric field and do not hinder the growth of induced domains in the macrodomain neighborhood.

The effect of charged domain boundaries is not limited to the electrophysical properties of crystals. It was found that reduction annealing in an oxygen free environment at a temperature that is known to be below the Curie point not only changes the color of the crystal and increases its electrical conductivity by producing color centers, but also changes its surface morphology. Along with the expected smoothing of the crystal topography [51, 52] due to recrystallization of the surface layer that was damaged and probably partially amorphized during specimen mechanical polishing, reduction annealing of an *x*-cut produced an elongated trench with a depth of ~0.5 nm and a width of ~1 μm coinciding with the charged head-to-head domain boundary. This trench can originate from a change in the recrystallization activation energy, deceleration of the lateral growth of the material and enhanced sublimation of the material at the domain boundary. Clarification of the origin of this phenomenon requires further investigation.

4. Conclusion

Local repolarization of ferroelectric domains in bidomain $LiNbO_3$ crystals with charged head-to-head and tail-to-tail domain walls was studied by applying electric potential to AFM cantilever. We observed polarization regularities and dependence of domain size on the polarity, duration and application point of electric potential. Screening of the growth of the induced domains by head-to-head domain boundaries was shown. Multi-beam domain growth in $LiNbO_3$ crystals after reduction annealing in an oxygen free environment was described.

Acknowledgments

The study was performed with financial support from the Russian Foundation for Basic Research, Project No. 18-32-00941.

Atomic force microscopy studies were carried out with financial support from the Ministry of Education and Science of the Russian Federation on premises of the Joint Use Center for Materials Science and Metallurgy of NUST MISiS within State Assignment (basic research, project #0718-2020-0031 “New magnetoelectric composite materials based on oxide ferroelectrics having an ordered domain structure: production and properties”).

References

1. Lengyel K., Péter Á., Kovács L., Corradi G., Pálfalvi L., Hebling J., Unferdorben M., Dravecz G., Hajdara I., Szaller Z., Polgár K. Growth, defect structure, and THz application of stoichiometric lithium niobate. *Appl. Phys. Rev.*, 2015; 2(4): 040601. https://doi.org/10.1063/1.4929917
2. Bazzan M., Fontana M. Preface to special topic: Lithium niobate properties and applications: reviews of emerging trends. *Appl. Phys. Rev.*, 2015; 2(4): 040501. https://doi.org/10.1063/1.4928590
3. Bazzan M., Sada C. Optical waveguides in lithium niobate: Recent developments and applications. *Appl. Phys. Rev.*, 2015; 2(4): 040603, https://doi.org/10.1063/1.4931601
4. Boes A., Corcoran B., Chang L., Bowers J., Mitchell A. Status and potential of lithium niobate on insulator (LNOI) for photonic integrated circuits. *Laser & Photonics Reviews*, 2018; 12(4): 1700256. https://doi.org/10.1002/lpor.201700256
5. Turutin A.V, Vidal J.V, Kubasov I.V, Kislyuk A.M., Malinkovich M.D., Parkhomenko Y.N., Kobeleva S.P., Kholkin A.L., Sobolev N.A. Low-frequency magnetic sensing by magnetoelectric metglas/bidomain $LiNbO_3$ long bars. *J. Phys. D: Appl. Phys.*, 2018; 51(21): 214001. https://doi.org/10.1088/1361-6463/aabda4
6. Kubasov I.V., Kislyuk A.M., Malinkovich M.D., Temirov A.A., Ksenich S.V., Kiselev D.A., Bykov A.S., Parkhomenko Y.N. A novel vibration sensor based on bidomain lithium niobate crystal. *Acta Phys. Polonica A*, 2018; 134(1): 106–108. https://doi.org/10.12693/APhysPolA.134.106
7. Zhukov R.N., Ksenich S.V., Kubasov I.V., Timushkin N.G., Temirov A.A., Kiselev D.A., Bykov A.S., Malinkovich M.D., Vygovskaya E.A., Toporova O.V. Studying local conductivity in LiNbO3 films via electrostatic force microscopy. *Bull. Russian Academy of Sciences: Phys.*, 2014; 78(11): 1223–1226. https://doi.org/10.3103/S106287381411029X
8. Kubasov I.V., Kislyuk A., Turutin A., Bykov A., Kiselev D., Temirov A., Zhukov R., Sobolev N., Malinkovich M., Parkhomenko Y.

Low-frequency vibration sensor with a sub-nm sensitivity using a bidomain lithium niobate crystal. *Sensors*, 2019; 19(3): 614. https://doi.org/10.3390/s19030614

9. Parkhomenko Y.N., Sobolev N.A., Kislyuk A.M., Kholkin A.L., Malinkovich M.D., Turutin A.V., Kobeleva S.P., Vidal J.V., Pakhomov O.V., Kubasov I. V. Magnetoelectric metglas/bidomain *y* + 140°-cut lithium niobate composite for sensing *fT* magnetic fields. *Appl. Phys. Lett.*, 2018; 112(26): 262906. https://doi.org/10.1063/1.5038014
10. Vidal J.V., Turutin A.V., Kubasov I.V., Malinkovich M.D., Parkhomenko Y.N., Kobeleva S.P., Kholkin A.L., Sobolev N.A. Equivalent magnetic noise in magnetoelectric laminates comprising bidomain $LiNbO_3$ crystals. *IEEE Transactions on Ultrasonics, Ferroelectrics, and Frequency Control*, 2017; 64(7): 1102–1119. https://doi.org/10.1109/TUFFC.2017.2694342
11. Kubasov I.V., Kislyuk A.M., Malinkovich M.D., Temirov A.A., Ksenich S.V., Kiselev D.A., Bykov A.S., Parkhomenko Y.N. Vibrational Power Harvester Based on Lithium Niobate Bidomain Plate. *Acta Phys. Polonica A*, 2018; 134(1): 90–92. https://doi.org/10.12693/APhysPolA.134.90
12. Chen F., Kong L., Song W., Jiang C., Tian S., Yu F., Qin L., Wang C., Zhao X. The electromechanical features of $LiNbO_3$ crystal for potential high temperature piezoelectric applications. *J. Materiomics*, 2019; 5(1): 73–80. https://doi.org/10.1016/j.jmat.2018.10.001
13. Esin A.A., Akhmatkhanov A.R., Shur V.Y. Tilt control of the charged domain walls in lithium niobate. *Appl. Phys. Lett*., 2019; 114(9): 092901. https://doi.org/10.1063/1.5079478
14. Neradovskaia E.A., Neradovskiy M.M., Esin A.A., Chuvakova M.A., Baldil P., De Micheli M.P., Akhmatkhanov A.R., Forget N., Shur V.Y. Domain kinetics during polarization reversal in 36° Y-cut congruent lithium niobate. *IOP Conference Series: Materials Science and Engineering*, 2018; 443: 012024. https://doi.org/10.1088/1757-899X/443/1/012024
15. Campbell M.P., McConville J.P.V., McQuaid R.G.P., Prabhakaran D., Kumar A., Gregg J.M. Hall effect in charged conducting ferroelectric domain walls. *Nature Communications*, 2016; 7(1): 13764. https://doi.org/10.1038/ncomms13764
16. Kuroda A., Kurimura S., Uesu Y. Domain inversion in ferroelectric MgO:$LiNbO_3$ by applying electric fields. *Appl. Phys. Lett.*, 1996; 69(11): 1565–1567. https://doi.org/10.1063/1.117031
17. Wolba B., Seidel J., Cazorla C., Godau C., Haußmann A., Eng L.M. Resistor network modeling of conductive domain walls in lithium niobate. *Advanced Electronic Materials*, 2018; 4(1): 1700242. https://doi.org/10.1002/aelm.201700242
18. Gureev M.Y., Tagantsev A.K., Setter N. Head-to-head and tail-to-tail 180° domain walls in an isolated ferroelectric. *Phys. Rev. B*, 2011; 83(18): 184104. https://doi.org/10.1103/PhysRevB.83.184104
19. Strukov B.A., Levanyuk A.P. *Ferroelectric Phenomena in Crystals*. Berlin; Heidelberg: Springer, 1998. https://doi.org/10.1007/978-3-642-60293-1
20. Tasson M., Legal H., Peuzin J.C., Lissalde F.C. Mécanismes d'orientation de la polarisation spontanée dans le niobate de lithium au voisinage du point de Curie. *Phys. Status Solidi (a)*, 1975; 31(2): 729–737. https://doi.org/10.1002/pssa.2210310246
21. Tasson M., Legal H., Gay J.C., Peuzin J.C., Lissalde F.C. Piezoelectric study of poling mechanism in lithium niobate crystals at temperature close to the curie point. *Ferroelectrics*, 1976; 13(1): 479–481. https://doi.org/10.1080/00150197608236646
22. Bykov A.S., Grigoryan S.G., Zhukov R.N., Kiselev D.A., Ksenich S.V., Kubasov I.V., Malinkovich M.D., Parkhomenko Y.N. Formation of bidomain structure in lithium niobate plates by the stationary external heating method. *Russian Microelectronics*, 2014; 43(8): 536–542. https://doi.org/10.1134/S1063739714080034
23. Kubasov I.V., Kislyuk A.M., Bykov A.S., Malinkovich M.D., Zhukov R.N., Kiselev D.A., Ksenich S.V., Temirov A.A., Timushkin N.G., Parkhomenko Y.N. Bidomain structures formed in lithium niobate and lithium tantalate single crystals by light annealing. *Crystallography Reports*, 2016; 61(2): 258–262. https://doi.org/10.1134/S1063774516020115
24. Kubasov I.V., Timshina M.S., Kiselev D.A., Malinkovich M.D., Bykov A.S., Parkhomenko Y.N. Interdomain region in single-crystal lithium niobate bimorph actuators produced by light annealing. *Crystallography Reports*, 2015; 60(5): 700–705. https://doi.org/10.1134/S1063774515040136
25. Ohnishi N. An etching study on a heat-induced layer at the positive-domain surface of $LiNbO_3$. *Jpn. J. Appl. Phys*., 1977; 16(6): 1069–1070. https://doi.org/10.1143/JJAP.16.1069
26. Nakamura K., Ando H., Shimizu H. Partial domain inversion in $LiNbO_3$ plates and its applications to piezoelectric devices. *IEEE 1986 Ultrasonics Symposium*, 1986: 719–722. https://doi.org/10.1109/ULTSYM.1986.198828
27. Nakamura K., Ando H., Shimizu H. Ferroelectric domain inversion caused in $LiNbO_3$ plates by heat treatment. *Appl. Phys. Lett.*, 1987; 50(20): 1413–1414. https://doi.org/10.1063/1.97838
28. Nakamura K., Ando H., Shimizu H. Shimizu H. Bending vibrator consisting of a $LiNbO_3$ plate with a ferroelectric inversion layer. *Jpn. J. Appl. Phys.*, 1987; 26(S2): 198. https://doi.org/10.7567/JJAPS.26S2.198
29. Nakamura K., Shimizu H. Hysteresis-free piezoelectric actuators using $LiNbO_3$ plates with a ferroelectric inversion layer. *Ferroelectrics*, 1989; 93(1): 211–216. https://doi.org/10.1080/00150198908017348
30. Nakamura K., Nakamura T., Yamada K. Torsional actuators using $LiNbO_3$ plates with an inversion layer. *Jpn. J. Appl. Phys.*, 1993; 32(5B): 2415–2417. https://doi.org/10.1143/JJAP.32.2415
31. Rosenman G., Kugel V.D., Shur D. Diffusion-induced domain inversion in ferroelectrics. *Ferroelectrics*, 1995; 172(1): 7–18. https://doi.org/10.1080/00150199508018452
32. Ievlev A.V., Alikin D.O., Morozovska A.N., Varenyk O.V., Eliseev E.A., Kholkin A.L., Shur V.Y., Kalinin S.V. Symmetry breaking and electrical frustration during tip-induced polarization switching in the nonpolar cut of lithium niobate single crystal. *ACS Nano*, 2015; 9(1): 769–777. https://doi.org/10.1021/nn506268g
33. Alikin D.O., Ievlev A.V., Turygin A.P., Lobov A.I., Kalinin S.V., Shur V.Y. Tip-induced domain growth on the non-polar cuts of lithium niobate single-crystals. *Appl. Phys. Lett.*, 2015; 106(18): 182902. https://doi.org/10.1063/1.4919872
34. Morozovska A.N., Ievlev A.V., Obukhovskii V.V., Fomichov Y., Varenyk O.V., Shur V.Y., Kalinin S.V., Eliseev E.A. Self-consistent theory of nanodomain formation on nonpolar surfaces of ferroelectrics. *Phys. Rev. B*, 2016; 93(16): 165439. https://doi.org/10.1103/PhysRevB.93.165439
35. Starkov A.S., Starkov I.A. Dependence of the ferroelectric domain shape on the electric field of the microscope tip. *J. Appl. Phys.*, 2015; 118(7): 072010. https://doi.org/10.1063/1.4927800
36. Morozovska A.N., Eliseev E.A., Kalinin S.V. Domain nucleation and hysteresis loop shape in piezoresponse force spectroscopy. *Appl. Phys. Lett.*, 2006; 89(19): 192901. https://doi.org/10.1063/1.2378526

37. Turygin A., Alikin D., Alikin Y., Shur V. The formation of self-organized domain structures at non-polar cuts of lithium niobate as a result of local switching by an SPM tip. *Materials*, 2017; 10(10): 1143. https://doi.org/10.3390/ma10101143
38. Strelcov E., Ievlev A.V., Jesse S., Kravchenko I.I., Shur V.Y., Kalinin S.V. Direct probing of charge injection and polarization-controlled ionic mobility on ferroelectric $LiNbO_3$ surfaces. *Advanced Materials*, 2014; 26(6): 958–963. https://doi.org/10.1002/adma.201304002
39. Bordui P.F., Jundt D.H., Standifer E.M., Norwood R.G., Sawin R.L., Galipeau J.D. Chemically reduced lithium niobate single crystals: Processing, properties and improved surface acoustic wave device fabrication and performance. *J. Appl. Phys.*, 1999; 85(7): 3766–3769. https://doi.org/10.1063/1.369775
40. Dhar A., Singh N., Singh R.R.K., Singh R.R.K. Low temperature dc electrical conduction in reduced lithium niobate single crystals. *J. Phys. Chem. Solids*, 2013; 74(1): 146–151. https://doi.org/10.1016/j.jpcs.2012.08.011
41. Pawlik A.-S., Kämpfe T., Haußmann A., Woike T., Treske U., Knupfer M., Büchner B., Soergel E., Streubel R., Koitzsch A., Eng L.M. Polarization driven conductance variations at charged ferroelectric domain walls. *Nanoscale*, 2017; 9(30): 10933–10939. https://doi.org/10.1039/C7NR00217C
42. Ievlev A.V., Morozovska A.N., Shur V.Y., Kalinin S.V. Ferroelectric switching by the grounded scanning probe microscopy tip. *Phys. Rev. B*, 2015; 91(21): 214109. https://doi.org/10.1103/PhysRevB.91.214109
43. Turygin A.P., Alikin D.O., Kosobokov M.S., Ievlev A.V., Shur V.Y. Self-organized formation of quasi-regular ferroelectric nanodomain structure on the nonpolar cuts by grounded SPM tip. *ACS Applied Materials & Interfaces*, 2018; 10(42): 36211–36217. https://doi.org/10.1021/acsami.8b10220
44. Jösch W., Munser R., Ruppel W., Würfel P. The photovoltaic effect and the charge transport in $LiNbO_3$. *Ferroelectrics*, 1978; 21(1): 623–625. https://doi.org/10.1080/00150197808237347
45. Werner C.S., Herr S.J., Buse K., Sturman B., Soergel E., Razzaghi C., Breunig I. Large and accessible conductivity of charged domain walls in lithium niobate. *Scientific Reports*, 2017; 7(1): 9862. https://doi.org/10.1038/s41598-017-09703-2
46. Volk T., Wöhlecke M. Lithium Niobate, Berlin; Heidelberg: Springer, 2008. https://doi.org/10.1007/978-3-540-70766-0
47. Chien C.L., Westgate C.R.(Eds.) The Hall Effect and Its Applications. Boston (MA): Springer, 1980. https://doi.org/10.1007/978-1-4757-1367-1
48. Dhar A., Mansingh A. On the correlation between optical and electrical properties in reduced lithium niobate crystals. *J. Phys. D: Appl. Phys.*, 1991; 24(9): 1644–1648. https://doi.org/10.1088/0022-3727/24/9/019
49. Imlau M., Badorreck H., Merschjann C. Optical nonlinearities of small polarons in lithium niobate. *Appl. Phys. Rev.*, 2015; 2(4): 040606. https://doi.org/10.1063/1.4931396
50. Yatsenko A.V., Yevdokimov S.V., Pritulenko A.S., Sugak D.Y., Solskii I.M. Electrical properties of $LiNbO_3$ crystals reduced in a hydrogen atmosphere. *Phys. Solid State*, 2012; 54(11): 2231–2235. https://doi.org/10.1134/S1063783412110339
51. Saito A., Matsumoto H., Ohnisi S., Akai-Kasaya M., Kuwahara Y., Aono M. Structure of atomically smoothed $LiNbO_3$ (0001) surface. *Jpn. J. Appl. Phys.*, 2004; 43(4B): 2057–2060. https://doi.org/10.1143/JJAP.43.2057
52. Sanna S., Schmidt W.G. $LiNbO_3$ surfaces from a microscopic perspective. *J. Phys.: Condensed Matter*, 2017; 29(41): 413001. https://doi.org/10.1088/1361-648X/aa818d